

Unconventional structure-assisted optical manipulation of high-index nanowires in liquid crystals

David Engström,^{1,2} Michael C.M. Varney,^{1,3} Martin Persson,^{1,2} Rahul P. Trivedi,^{1,3} Kris A. Bertness,⁴ Mattias Goksör,² and Ivan I. Smalyukh^{1,3,5,*}

¹Department of Physics, University of Colorado, Boulder, Colorado 80309, USA

²Department of Physics, University of Gothenburg, SE-412 96 Göteborg, Sweden

³Liquid Crystal Materials Research Center, Department of Electrical, Computer, and Energy Engineering, and Materials Science and Engineering Program, University of Colorado, Boulder, Colorado 80309, USA

⁴National Institute of Standards and Technology, Boulder, Colorado 80305, USA

⁵Renewable and Sustainable Energy Institute, National Renewable Energy Laboratory and University of Colorado, Boulder, Colorado 80309, USA

*Ivan.Smalyukh@colorado.edu

Abstract: Stable optical trapping and manipulation of high-index particles in low-index host media is often impossible due to the dominance of scattering forces over gradient forces. Here we explore optical manipulation in liquid crystalline structured hosts and show that robust optical manipulation of high-index particles, such as GaN nanowires, is enabled by laser-induced distortions in long-range molecular alignment, via coupling of translational and rotational motions due to helicoidal molecular arrangement, or due to elastic repulsive interactions with confining substrates. Anisotropy of the viscoelastic liquid crystal medium and particle shape give rise to a number of robust unconventional trapping capabilities, which we use to characterize defect structures and study rheological properties of various thermotropic liquid crystals.

©2012 Optical Society of America

OCIS codes: (140.7010) Laser trapping; (160.3710) Liquid crystals; (160.4236) Nanomaterials; (180.6900) Three-dimensional microscopy.

References and links

1. D. G. Grier, "A revolution in optical manipulation," *Nature* **424**(6950), 810–816 (2003).
2. S. Bayouh, T. A. Nieminen, N. R. Heckenberg, and H. Rubinsztein-Dunlop, "Orientation of biological cells using plane-polarized Gaussian beam optical tweezers," *J. Mod. Opt.* **50**, 1581 (2003).
3. K. C. Neuman and S. M. Block, "Optical trapping," *Rev. Sci. Instrum.* **75**(9), 2787–2809 (2004).
4. A. Ashkin, J. M. Dziedzic, J. E. Bjorkholm, and S. Chu, "Observation of a single-beam gradient force optical trap for dielectric particles," *Opt. Lett.* **11**(5), 288–290 (1986).
5. K. Dholakia and T. Čížmár, "Shaping the future of manipulation," *Nat. Photonics* **5**(6), 335–342 (2011).
6. E. Higurashi, H. Ukita, H. Tanaka, and O. Ohguchi, "Optically induced rotation of anisotropic micro-objects fabricated by surface micromachining," *Appl. Phys. Lett.* **64**(17), 2209–2210 (1994).
7. R. C. Gauthier, M. Ashman, and C. P. Grover, "Experimental confirmation of the optical-trapping properties of cylindrical objects," *Appl. Opt.* **38**(22), 4861–4869 (1999).
8. W. Singer, T. A. Nieminen, U. J. Gibson, N. R. Heckenberg, and H. Rubinsztein-Dunlop, "Orientation of optically trapped nonspherical birefringent particles," *Phys. Rev. E Stat. Nonlin. Soft Matter Phys.* **73**(2), 021911 (2006).
9. H. Ukita and K. Nagatomi, "Theoretical demonstration of a newly designed micro-rotator driven by optical pressure on a eight incident surface," *Opt. Rev.* **4**(4), 447–449 (1997).
10. D. B. Phillips, D. M. Carberry, S. H. Simpson, H. Schäfer, M. Steinhart, R. Bowman, G. M. Gibson, M. J. Padgett, S. Hanna, and M. J. Miles, "Optimizing the optical trapping stiffness of holographically trapped microrods using high-speed video tracking," *J. Opt.* **13**(4), 044023 (2011).
11. S. H. Simpson and S. Hanna, "Holographic optical trapping of microrods and nanowires," *J. Opt. Soc. Am. A* **27**(6), 1255–1264 (2010).
12. S. H. Simpson and S. Hanna, "Optical trapping of microrods: variation with size and refractive index," *J. Opt. Soc. Am. A* **28**(5), 850–858 (2011).

13. C. P. Lapointe, T. G. Mason, and I. I. Smalyukh, "Shape-controlled colloidal interactions in nematic liquid crystals," *Science* **326**(5956), 1083–1086 (2009).
14. J. E. Curtis, B. A. Koss, and D. G. Grier, "Dynamic holographic optical tweezers," *Opt. Commun.* **207**(1-6), 169–175 (2002).
15. D. Engström, R. P. Trivedi, M. Persson, M. Goksör, K. A. Bertness, and I. I. Smalyukh, "Three-dimensional imaging of liquid crystal structures and defects by means of holographic manipulation of colloidal nanowires with faceted sidewalls," *Soft Matter* **7**(13), 6304–6312 (2011).
16. R. P. Trivedi, D. Engström, and I. I. Smalyukh, "Optical manipulation of colloids and defect structures in anisotropic liquid crystal fluids," *J. Opt.* **13**(4), 044001 (2011).
17. K. A. Bertness, A. Roshko, N. A. Sanford, J. M. Barker, and A. Davydov, "Spontaneously grown GaN and AlGaIn nanowires," *J. Cryst. Growth* **287**(2), 522–527 (2006).
18. Certain commercial materials are identified in this paper only to specify experimental procedures. Such identification implies neither recommendation or endorsement by the National Institute of Standards and Technology, nor that materials identified are necessarily the best available for the purpose.
19. B.-W. Lee and N. A. Clark, "Alignment of liquid crystals with patterned isotropic surfaces," *Science* **291**(5513), 2576–2580 (2001).
20. I. I. Smalyukh, S. V. Shiyonovskii, and O. D. Lavrentovich, "Three-dimensional imaging of orientational order by fluorescence confocal polarizing microscopy," *Chem. Phys. Lett.* **336**(1-2), 88–96 (2001).
21. V. L. Y. Loke, M. P. Mengüç, and T. A. Nieminen, "Discrete dipole approximation with surface interaction: Computational toolbox for MATLAB," *J. Quant. Spectrosc. Radiat. Transf.* **112**(11), 1711–1725 (2011).
22. T. A. Nieminen, V. L. Y. Loke, A. B. Stilgoe, G. Knöner, A. M. Brańczyk, N. R. Heckenberg, and H. Rubinsztein-Dunlop, "Optical tweezers computational toolbox," *J. Opt. A, Pure Appl. Opt.* **9**(8), S196–S203 (2007).
23. V. M. Pergamenschchik and V. A. Uzunova, "Colloid-wall interaction in a nematic liquid crystal: the mirror-image method of colloidal nematostatics," *Phys. Rev. E Stat. Nonlin. Soft Matter Phys.* **79**(2), 021704 (2009).
24. A. Ortega and J. G. de la Torre, "Hydrodynamic properties of rodlike and disklike particles in dilute solution," *J. Chem. Phys.* **119**(18), 9914–9919 (2003).
25. C. J. Smith and C. Denniston, "Elastic response of a nematic liquid crystal to an immersed nanowire," *J. Appl. Phys.* **101**(1), 014305 (2007).
26. R. Di Leonardo, E. Cammarota, G. Bolognesi, H. Schäfer, and M. Steinhart, "Three-dimensional to two-dimensional crossover in the hydrodynamic interactions between micron-scale rods," *Phys. Rev. Lett.* **107**(4), 044501 (2011).
27. Q. Liu, T. Asavei, T. Lee, H. Rubinsztein-Dunlop, S. He, and I. I. Smalyukh, "Measurement of viscosity of lyotropic liquid crystals by means of rotating laser-trapped microparticles," *Opt. Express* **19**(25), 25134–25143 (2011).
28. H. F. Gleeson, T. A. Wood, and M. Dickinson, "Laser manipulation in liquid crystals: an approach to microfluidics and micromachines," *Philos. Transact. A Math. Phys. Eng. Sci.* **364**(1847), 2789–2805 (2006).

1. Introduction

Optical trapping is a non-contact manipulation technique broadly used in science fields ranging from condensed matter physics to biology and biomedicine, as well as for various technological applications [1–3]. Stable manipulation typically uses tightly focused laser beams that exert optical gradient forces and pull particles towards the maximum-intensity region of the focal plane and overcome scattering forces that tend to push the particle along the light-propagation direction [4]. This imposes restrictions on the refractive indices of the particles with respect to the fluid host media, specifically that the refractive index of particles has to be modestly higher than that of the medium. Particle shape is another factor that determines trapping stability, orientation, and possible rotation/motion of particles within the trap [1–9]. For example, colloidal cylinders with dimensions comparable to or smaller than the wavelength of the trapping laser spontaneously align along either the beam propagation or linear polarization directions [7,8] while larger anisotropic microparticles can be trapped in desired orientations using multiple traps [10–12] or optical vortex beams [13]. Some of the remaining challenges include stable trapping of particles with a refractive index much larger than that of the surrounding host medium, manipulation of non-spherical particles while aligning them in desired orientations, as well as robust control of colloidal inclusions in anisotropic fluid hosts such as liquid crystals (LCs).

In our work, we explore optical manipulation of high-index GaN nanowires infused in nematic and cholesteric LCs in the regime when optical gradient forces are much weaker than scattering forces. We show that stable non-contact optical manipulation of these particles is

still possible because of the structured LC self-organization and its response to laser beams. Laser manipulation properties are studied as a function of laser power, structure of long-range molecular alignment (described by the director field $\mathbf{N}(\mathbf{r})$), and LC confinement conditions. This robust structure-assisted trapping allows us to characterize three-dimensional (3D) defect morphology and local rheological properties of LCs.

2. Optical setup

Our setup (Fig. 1) combines holographic optical tweezers (HOT) [14] with fluorescence confocal polarizing microscopy (FCPM) [15,16] and allows for simultaneous optical 3D manipulation and imaging of a variety of systems. The HOT is built around an electrically addressed liquid-crystal spatial light modulator (LC-SLM) with 512×512 pixels (BNS XY series P512-1064, with each pixel being $15 \mu\text{m} \times 15 \mu\text{m}$). Two telescopes, one before and another after the SLM, resize the beam to overfill the active area of the SLM and image the SLM on the back-aperture of the objective, respectively. While trapping is performed at 1064 nm, the sample imaging in 3D is done via dye excitation at 488 nm and fluorescence detection in the range of 505–525 nm. Both the HOT and the FCPM use the same oil immersion objective. The used objectives with $60 \times$ and $100 \times$ magnification had numerical aperture of 1.42. In addition to laser manipulation and confocal microscopy, this setup allows us to perform conventional polarizing optical microscopy (POM) studies.

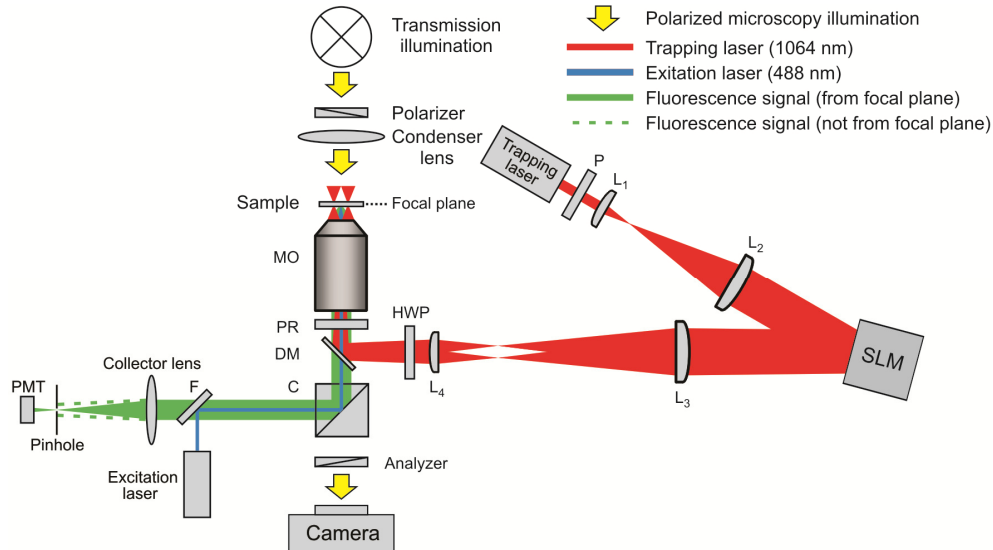


Fig. 1. Integrated HOT and FCPM setup. The HOT part of the setup is composed of a laser ($\lambda = 1064 \text{ nm}$), plano-convex lenses L_1 (focal length 100 mm), L_2 (250 mm), L_3 (850 mm), and L_4 (400 mm) with anti-reflection coating, a Glan-Laser polarizer (P), a half-wave plate (HWP), a dichroic mirror (DM), a polarization rotator (PR), and a microscope objective (MO). The FCPM consists of an excitation laser, a dichroic filter (F), a beam-splitting cube (C), a pinhole, and a photomultiplier tube (PMT). The setup also allows for POM imaging.

3. Sample and cell preparation

Figures 2(a), 2(b) shows representative GaN nanowires grown via molecular beam epitaxy [17]. The method yields nanowires with a hexagonal cross-section of $\sim 300 \text{ nm}$ in width. Ultrasonic removal of the nanowires from the growth substrate into a solvent (isopropanol) results in a fairly monodisperse solution with a typical nanowire length of $\sim 10 \mu\text{m}$. Our study utilized LC mixtures such as the nematic LC (NLC) E31, and a cholesteric LC (CLC) composed of an NLC host (e.g., E7, ZLI-3412, or ZLI-2806) mixed with a chiral agent (CB-15) [15,18]. E31 is a mixture of cyanobiphenyl homologs, with elastic constants of bend,

splay, and twist being $K_{33} = 25\text{pN}$, $K_{11} = 17.5\text{pN}$, and $K_{22} = 8.5\text{pN}$, respectively [19]. For FCPM imaging, our samples were doped with a tiny amount (0.01 wt. %) of a fluorescent dye *n,n'*-bis(2,5-di-*tert*-butylphenyl)-3,4,9,10-perylenedicarboximide (BTBP, Aldrich) that yields a strong fluorescence signal without affecting LC properties [20]. LC cells are fabricated with two glass substrates sandwiched together by the use of UV curable glue (Norland optical adhesive NOA-63). Silica spheres mixed with glue set a cell gap ranging from 10 μm to 60 μm . Spin-coated thin films of polyvinyl alcohol (PVA) are used as surface alignment layers; PVA coatings on the opposite inner surfaces of confining glass plates are rubbed in the anti-parallel fashion before cell assembly to provide unidirectional planar surface anchoring. The nanowire solution is mixed into an LC sample via solvent exchange, after which the solvent is evaporated. This nanowire-LC dispersion is then infused into the cell in its nematic phase by means of capillary forces. Finally, the cell is sealed with fast curing epoxy.

4. Optical manipulation of nanowires in nematic liquid crystals

In a planar-aligned NLC, nanowires tend to align themselves parallel to the uniform far-field director \mathbf{N}_0 to minimize elastic energy, Figs. 2(c)-2(e). Due to a director pre-tilt induced by anti-parallel surface rubbing of the PVA alignment layer, nanowires commonly tilt out of the (*x*-*y*) plane at an angle < 8 degrees. POM images indicate that the nanowires weakly distort the director field, with areas of the strongest distortions occurring at their ends, Fig. 2(c). Heating of the surrounding LC during optical manipulation of nanowires is negligible because of their low absorption coefficient of $\sim 80\text{ cm}^{-1}$ at the laser wavelength of 1064 nm.

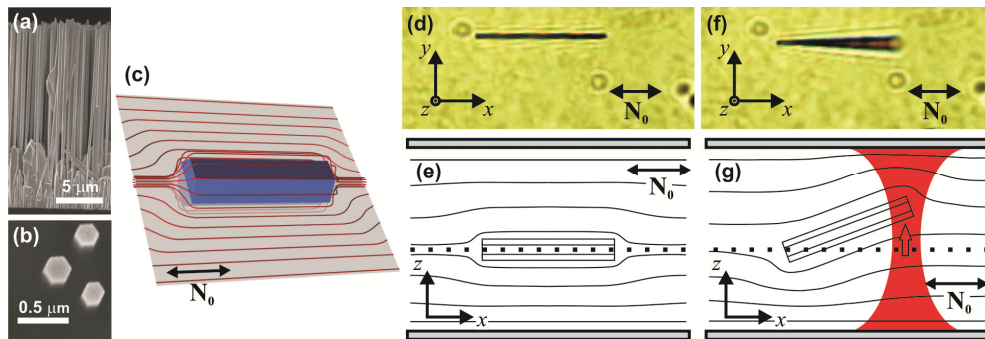


Fig. 2. Nanowires in NLCs. (a) and (b) SEM micrographs of (a) the side-view and (b) cross-sections of GaN nanowires. (c) Schematic of $\langle \mathbf{N} \rangle(\mathbf{r})$ around a hexagonal faceted nanowire in an aligned NLC. (d) Micrograph and (e) schematic of $\langle \mathbf{N} \rangle(\mathbf{r})$ around a nanowire in an aligned NLC. (f) Micrograph and (g) schematic of $\langle \mathbf{N} \rangle(\mathbf{r})$ around a nanowire under the influence of a laser trap (light is propagating in the positive *z*-direction) centered at one of nanowire ends. The dotted lines in (e) and (g) indicate the image plane used to capture the micrographs shown in (d) and (f).

A laser beam of power $< 25\text{ mW}$ initially attracts a nearby nanowire. However, once the nanowire overlaps with the focused laser beam, it is pushed along the light propagation direction, indicating that the high refractive index contrast between the nanowire ($n_{\text{GaN}} = 2.4$) and the LC ($n_{\text{LC}} \approx 1.5$) precludes stable 3D trapping. This is true regardless of trap position and beam polarization relative to the director or nanowire. This hypothesis is supported by numerical simulations, using the T-matrix method and a discrete-dipole approximation [21,22], yielding a strong force of 30–80 pN in the positive *z*-direction. A trap positioned on one end of the nanowire rotates the nanowire out of the (*x*,*y*)-plane to an angle at which the optical torque, due to scattering force acting on one of the nanowire's ends, is balanced by the elastic torque tending to align the nanowire along \mathbf{N}_0 . Its initial orientation is restored when the beam is turned off. Elastic distortions around the rotated nanowire are of monopole type and mediate repulsive elastic interactions of the colloid with the strong surface boundary conditions of the confining substrates. These interactions can be modeled using the method of

images, analogous to that used in electrostatics [23]. Interactions between elastic monopoles induced by rotated nanowires with their image monopoles on the opposite sides of the LC-substrate interfaces are repulsive [23] and are expected to slowly decay with distance d from the substrate as $\propto 1/d^2$. This assures that the optical scattering force is balanced by the elastic force of nanowire's repulsive interaction with the confining plates that tend to localize it in the cell midplane. Once the focused beam is removed, the elastic torque acting on the nanowire aligns the nanowire such that it returns to its initial orientation, again parallel to \mathbf{N}_0 , Figs. 2(d), 2(e).

Using an optical power of up to 20 mW, we have measured a maximum nanowire tilt angle of ~ 10 degrees from \mathbf{N}_0 , yielding an estimate of the axial optical force consistent with our numerical calculations. Thus, an optically tilted nanowire can be stably localized in the LC cell close to its midplane, due to the balance of scattering and gradient forces augmented with elastic repulsive forces between a rotated nanowire and confining plates. On the other hand, when a trap is positioned in the middle of the nanowire rather than at one of its ends, there is no elastic torque, and the weak elastic distortions around the colloid remain quadrupolar (Fig. 2(e)). This results in much weaker nanowire-substrate elastic interactions (with the force decaying as $\propto 1/d^6$) and an apparent pushing of the nanowire to the opposite substrate of the cell by the optical force. Thus, this type of elasticity- and confinement-assisted trapping has a number of limitations on cell thickness and trap position along nanowire for which stable 3D trapping is achieved.

At optical powers of about 35 mW and higher, laser traps realign the local director $\mathbf{N}(\mathbf{r})$ [16]. Thus, in addition to particle manipulation by optical forces, it is also possible to utilize the ensuing elastic forces to enable stable trapping of a GaN nanowire. Such trapping is accomplished when the trap polarization is orthogonal to \mathbf{N}_0 and the trap is turned on after being centered on the nanowire. By the use of this type of trap activation, multiple traps can be used to manipulate the nanowire at any point along its length. On the other hand, traps activated in close vicinity of the nanowire do not result in a stable trapping as the particle is repelled from a trap. These observations may be understood by considering the elastic energy cost of a laser-induced elastic distortion in the NLC, which is minimized when a trap is centered on the nanowire due to the volume of NLC with laser-induced distortions excluded by the presence of the nanowire. Due to tangential surface boundary conditions along the length of the rather long nanowire, it is typically repelled from the laser trap located nearby, again to minimize the elastic free energy. Clearly, this behavior at high laser powers is very different from that at low powers discussed above.

Figure 3(a) shows a nanowire manipulated by a single trap with laser power higher than the realignment threshold of 35 mW positioned at its left end. The trap, and consequently the end of the nanowire, is translated orthogonal to \mathbf{N}_0 at a constant rate of $0.5 \mu\text{m/s}$, while elastic forces retain its alignment along \mathbf{N}_0 . Figure 3(b) shows a similar experiment, where in addition to the moving trap, a stationary trap is positioned at the right end of the nanowire. As the left side trap is translated nearly orthogonal to \mathbf{N}_0 , the two traps are strong enough to overcome elastic forces, resulting in an in-plane rotation β_{nw} . At $\beta_{\text{nw}} \sim 13$ degrees, the right end of the nanowire escapes the trap and the nanowire rotates back to become parallel to \mathbf{N}_0 under the action of an elastic torque exerted by the NLC medium. The escape angle is experimentally observed to increase with increasing laser power, and is expected to depend on elastic and viscous properties of the NLC, and the angular velocity of trap motion, because both elastic and viscous torques oppose rotation of the nanowire away from the equilibrium alignment direction.

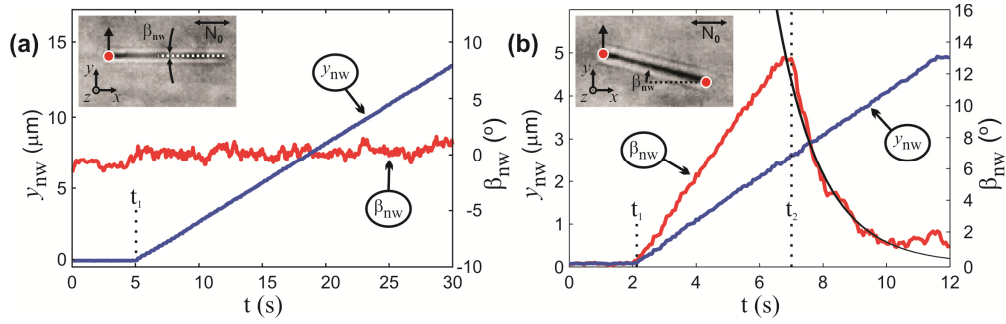


Fig. 3. Manipulation of a GaN nanowire in an NLC using high-power laser traps. (a) Nanowire manipulated by a single trap positioned at its left end (Media 1): at elapsed time $t_1 = 5.0$ s, the trap starts moving with a constant velocity. The inset shows a frame from the movie; \mathbf{N}_0 is along the x -axis. (b) Nanowire manipulated using two traps, one at each of its ends (Media 2): at elapsed time $t_1 = 2.1$ s, the left trap starts moving with a constant velocity while the right-end trap is immobile. At elapsed time $t_2 = 7.0$ s, the right end of the nanowire escapes its trap due to the elastic torque exerted by the NLC. Inset shows a frame from Media 2 at elapsed time 7.0 s; \mathbf{N}_0 is along the x -axis. In (a) and (b) graphs show nanowire's left end position y_{nw} and rotation angle β_{nw} vs. time. The black solid line in (b) is obtained by the use of the model and parameters $K = 13 \times 10^{-12}$ N, $\eta = 0.45$ P, $L_{nw} = 10$ μm , and $R_{nw} = 150$ nm. The cell gap is 60 μm .

Relaxation of the nanowire toward \mathbf{N}_0 is determined by the balance of elastic restoring and viscous drag forces, while inertial effects are negligible. The angular motion of the nanowire with a viscous drag of Stokes-sphere-equivalent volume is [24,25]

$$\beta(t) = c_1 e^{-\gamma t}, \quad (1)$$

where c_1 is determined by the escape angle and γ is the relaxation time constant:

$$\gamma = \frac{4}{3} \frac{K}{\eta L^2 \ln\left(2 \frac{L}{R}\right)} \left(\frac{L^2}{6R^2}\right)^{1/3}, \quad (2)$$

where K is the Frank elastic constant of the NLC in the “one-constant approximation”, L and R are the length and radius of a cylinder circumscribing the hexagonally-shaped nanowire, respectively, and η is an effective viscosity. Figure 3(b) shows the fit of this model to our data for known values for K and η , and experimentally measured L and R . The good agreement of our experiment shown in Fig. 3(b) with this model for known material parameters [19] suggests that simple manipulation of optically trapped nanowires can allow for microrheological measurements of Frank elastic constants and viscosities. These measurements might be done locally in sample regions of interest, e.g. in NLC droplets and near or within defect lines [26–28].

5. Optical manipulation of nanowires in cholesteric liquid crystals

A cholesteric LC infused into a cell with parallel surface rubbing results in a helical director structure that induces a strong coupling between a nanowire's z -position (z_{nw}) and its in-plane rotation angle (β_{nw}), Fig. 4(a). An optical beam focused on the center of a nanowire not only pushes the nanowire along the light-propagation direction but also forces it to rotate along the helical structure, as shown in Figs. 4(a)–4(f). The helical structure and CLC elasticity prevent the nanowire from tilting out of the (x, y) -plane, even when the trap is positioned at one of its ends. Since the z -component of the optical force (along the CLC helical axis) is balanced out by elastic forces preventing the nanowire tilt toward the helical axis, and since the rotations around and translations along the helical axis are mechanically coupled, optical manipulation

of the ends of a nanowire allows for robust manipulation of the nanowire in 3D. For controlled displacement of a nanowire within the (x,y) -plane, at least two focused laser beams are moved while the orientation of their center-to-center separation vector is kept fixed. For movement along the z -direction, one or two traps are positioned at each end of the nanowire and used to rotate the nanowire, resulting in a screw-like translation along the helical axis; it is somewhat easier to translate the nanowire along the direction of optical scattering force (away from the microscope objective) rather than opposed to it. This rotation-translation coupling allows for precise measurement of the local cholesteric pitch p , as shown in Fig. 4(g). Best fit of the experimental data of vertical z -position vs. the in-plane orientation angle, measured using a previously described method [15,16], yields cholesteric pitch of $p = 40.4 \pm 0.25 \mu\text{m}$ [15,16], which is consistent with the equilibrium pitch of the CLC used in our study.

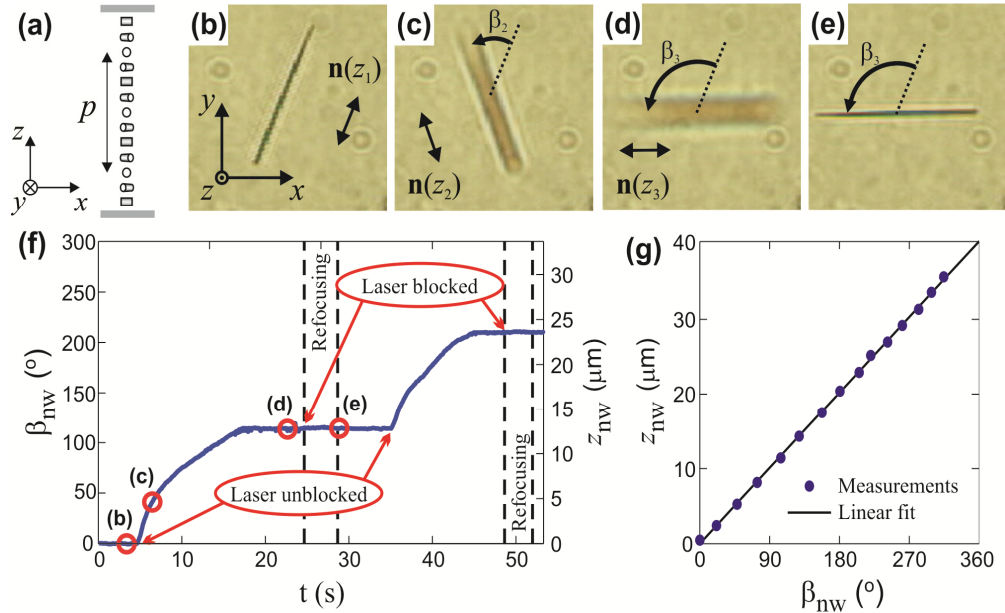


Fig. 4. Manipulation of GaN nanowires in a CLC. (a) Schematic of an equilibrium director structure in a CLC cell with pitch p . (b)–(e) Frames from [Media 3](#), in which a single focused optical beam, initially positioned on the center of a nanowire, forces the nanowire to rotate away from the microscope objective. The optical beam is then blocked, refocused, and unblocked at elapsed times of unblocking 4.5 s and 35.0 s. (f) Nanowire in-plane angle β_{nw} and z -position z_{nw} vs. time as extracted from [Media 3](#); Frames shown in (b)–(e) correspond to elapsed times indicated with red circles in (f). (g) Measured nanowire position z_{nw} as a function of the in-plane rotation angle β_{nw} . The cell gap is $60 \mu\text{m}$. A laser beam power of 50 mW at the sample plane was used in these experiments.

6. Trapping-assisted characterization of 3D defect morphology

There is a great interest in measuring and characterizing anisotropic properties and structure of LCs. Optical manipulation techniques demonstrated above give a simple and robust means for such measurements and also allow for mapping of complex director fields [15]. Figure 5 shows a nanowire manipulated in a CLC sample containing an “oily streak” defect at which cholesteric layers are discontinuous. By means of low-power manipulation, we have probed the CLC structure with a manipulated nanowire being used as a “compass” that always points along $\mathbf{N}(\mathbf{r})$. To demonstrate this, we have translated the nanowire above and below the oily streak defect along the x -direction, as shown in Fig. 5(d). The nanowire was also translated along a bent layer passing through the core of the oily streak, Fig. 5(c), revealing the director field in the vicinity and within this complex defect core. Similar non-contact manipulation

reveals the layered structure of the cholesteric LC sample and presence of various nonsingular and singular disclinations within the oily streak defect core (Fig. 5).

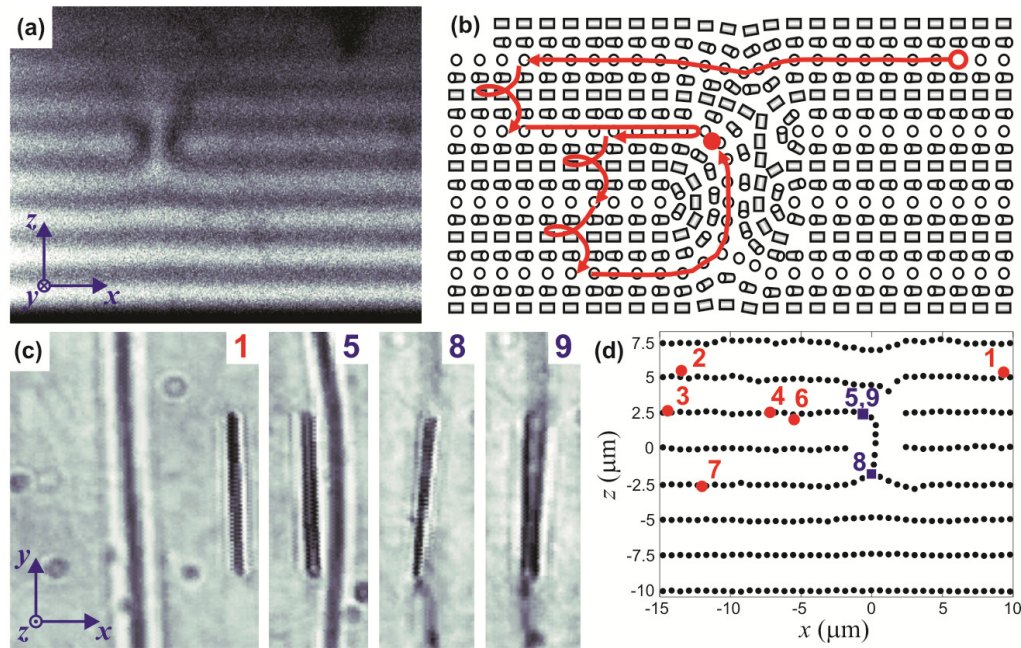


Fig. 5. GaN nanowire translated within and around an oily streak in a CLC. (a) FCPM vertical cross-section of the sample with an oily streak. (b) Schematic of the director structure around the defect with the nanowire translation trajectory (red line); the three rotated screws each indicate a 180° clock-wise rotation of the nanowire. (c) Frames from [Media 4](#) (sped up 2 times), [Media 5](#) (sped up 2 times), and [Media 6](#) (sped up 4 times) showing the nanowire being moved from position #1 to #2 in (d), the dislocation prohibiting the nanowire from moving across one of the broken layers, position #5 in (d), and the nanowire being pushed between positions #8 to #9 in (d), respectively. (d) Layered structure obtained using FCPM images shown with co-located nanowire positions measured using either in-plane FCPM images (red circles) or video microscopy frames (blue squares).

7. Conclusions

We have presented new approaches for unconventional structure-assisted optical manipulation of high-index nanowires in nematic and cholesteric liquid crystals. Stable 3D manipulation in these approaches is enabled by augmenting the optical gradient and scattering forces with forces due to trap-induced elastic distortions or by coupling of translational and rotational motions due to intrinsic helicoidal structures, or by elastic repulsive interactions with confining substrates when traps rotate nanowires and induce elastic monopole-like low-symmetry structures. Robust optical manipulation by above methods enables characterization of director structures, defect morphology, and local rheological properties of liquid crystals.

Acknowledgments

This work was supported by the International Institute for Complex Adaptive Matter (R.P.T., I.I.S.), and by NSF grants DMR-0820579 (R.P.T., I.I.S.), DMR-0844115 (R.P.T., I.I.S.), DMR-0645461 (I.I.S.), and DMR-0847782 (R.P.T., I.I.S.). D.E. acknowledges support of the Swedish Foundation for International Cooperation in Research and Higher Education. We thank T. Lee, V. Loke, T. Nieminen, B. Senyuk, and C. Twombly for discussions.